DESIGN AND CONTROL OF A SUPERCONDUCTING DC LINEAR MOTOR FOR ELECTROMAGNETIC LAUNCH SYSTEM

Guan Liu, Ji Li*
Engineering Research Center of Maglev Technology, National University of Defense Technology, Changsha, 410073, China

Abstract
A conventional AC linear machine for the electromagnetic launcher has a problem of low-efficiency. This paper presents a superconducting DC linear motor (SDCLM) to improve the energy-efficient of system for superhigh velocity electromagnetic launch. The operation principle and conception model are introduced. Detailed analytical formulas for magnetic force are presented. The static thrust versus position and dynamics launch process characteristics are simulated and computed. The result indicates that the superconducting DC linear motor offers outstanding efficiency merit as energy-efficient direct linear electric drives propelling large loading for electromagnetic launch system. Finally, a thrust control of superconducting DC linear motor (SDCLM) based on current compensation was proposed to minimum thrust fluctuant. The controller is designed based on the relationship between current and back-EMF, and the control scheme is assessed through simulation study.
Keywords: DC Linear Motor; Energy-Efficient; Large Loading; Electromagnetic Launch; Thrust Control; Current Compensation.

1. INTRODUCTION

Electromagnetic launch uses magnetic force to propel or drive objects based on the interaction between magnetic field and current. Compared with mechanical launch and chemical launch, electromagnetic launch offers such merits as higher launch efficiency, easy to control, reusable and large variety of launch structure. These advantages make electromagnetic launch have a promising application in aircraft launch, electromagnetic gun, aerospace launch assist, high speed test track and high speed train. At present, conventional electromagnetic launch models and systems can't achieve superhigh velocity with a heavy load because of limits of energy-efficient and power storage. The launch velocity of electromagnetic gun could reach up to 9600 m/s, but the mass of projectile is less than 100 kg [1]. The launch velocity of aircraft launch is around 103 m/s with a load of 22500 kg [2]-[4]. High speed maglev train could propel more than 30000 kg vehicle to 167.5 m/s by superconducting linear synchronous motor, but the acceleration is less than 1 m/s^2 [5]-[11]. So it's important to improve the energy-efficient of linear motor with the limitation of power storage.

To compensate the end-effect, rapidly-pulsed magnetic fields and segmented reaction are used to design high efficient linear induction motor [12]. And when permanent magnet and superconducting magnet are employed in the linear synchronous motor, a very high power factor can be obtained [13]-[14]. However electromagnetic launch is a dynamic progress without a steady operation point. It's impossible to keep a high power factor all along in a large acceleration path [15]. Because of the limitation of the power factor of ac linear motor, a concept of homopolar DC linear motor applied in electromagnetic launch was introduced. The system efficient of homopolar DC linear motor could achieve 75% [16]. And the results of study and experiments of a DC linear motor have verified good propulsion performances in high speed transportation system [17].

Except for high energy-efficient, linear propulsion drives for large loading electromagnetic launch system also have high-capacity. Superconducting magnet with high magnetic field would increase motor capacity. In recent years, the application research based on superconducting magnets has achieved distinct advance, thanks to the progress of producing techniques and overall performance in superconducting materials. It is successfully applied to high speed maglev train. The high speed test track at Holloman air force base was upgraded to superconducting electordynamic magnetic levitation in the mid-nineties. The superconducting magnet consists of a racetrack coil, which is lay-up wound with rectangular NbTi/Cu wire, and the peak field is 6.7 T. Two superconducting magnets, mounted on a sled, are propelled by solid fuel rocket motors. During six successfully flight tests, the sled has reached speeds of 186.9 m/s [18]-[23]. The similar superconducting magnet is applied in high speed maglev train in Japan, and the maximal operational speed is 167.5m/s [9], [10]. These successful applications indicate that superconducting magnet is available for superhigh velocity launch.

In this paper, the results of a design for a DC linear motor that uses superconducting magnet were present. The motor had been designed for use in large loading and superhigh velocity electromagnetic launch system. The structural design and theoretical analysis were described, and the dynamic characters of motor were evaluated. Finally, aiming at the problem that the thrust fluctuation of the air core motor, a thrust control based on current compensation is presented. The theoretical analysis and controller design were described, and the simulation results were released.

2. CONSTRUCTION AND PRINCIPLE OF OPERATION

The principle of two poles superconducting DC linear motor is presented in Fig. 1. It mainly includes a multi-winding ring armature coils and a moving field unit consisted of air core superconducting magnets. Air core motor with superconducting magnets is designed to break the upper limit of thrust in conventional iron-core motors. Because any further increasing in armature current will not results in an accompanying increase in the electromagnetic force generated by the saturated iron core. The ring winding is selected based on the following factors. When the linear motor is running at superhigh speed, a large pitch is often used to reduce the frequency of armature winding, which can reduce the requirement of the motor drive equipment. The pitch of superconducting linear synchronous motor is 1.35m on Yamanashi test line in Japan. When the armature winding frequency is 56.6Hz, the train running speed is 550Km/h. However, a large pitch of linear motor will make the end winding span is large. It will not only increase the resistance and inductance of armature winding , but also cause seriously overlap problem of armature winding. This increases the difficulty of armature winding manufacturing and limits the increasing in armature load. There is no overlap problem in the circumferential winding, which can further improve the electromotive force of the armature winding. And the end of the ring winding is short and reduce the end of the loss. In addition, the ring winding is easy to modular assembly and has good heat dissipation capability. However, the ring winding will make the motor electromechanical energy conversion capacity decline. The same size of the winding, the thrust of a linear motor with conventional winding is about 2.5 times the thrust of a linear motor with ring winding。The direction of the magnetic field is along with *y* axis. The armature current interacts with the magnetic field to produce propulsion force, as shown in Fig. 1. The force pushes the loading and accelerates it to a superhigh speed.

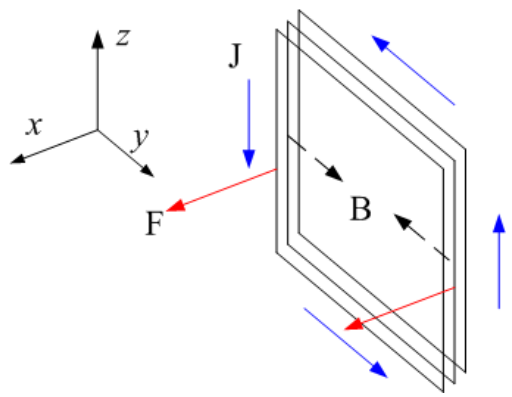

Fig.1. Principle of a SDCLM.

The superconducting magnet, mounted on a carrier, consists of a superconducting coil and a cooling vessel. Superconducting coil is cooled in the vessel. Before launch, the charge cables are retracted from power. A persistent switch is installed in the magnet bore to maintain the current flow while the power leads are disconnected from the magnet [21]. It makes superconducting magnet work like a permanent magnet without brush, but superconducting magnet could produce stronger magnetic filed than permanent magnet. The magnetic filed direction of two superconducting magnet are opposite, so the two superconducting magnets can produce the same direction thrust.

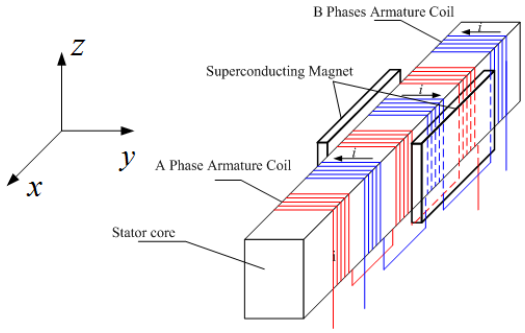

Fig.2. Fundamental Construction of SMDCLM.

The stator core is made of nonmagnetic material instead of ferromagnetic materials to avoid the problem of saturation of the permeable materials. Armature coils are regular flat copper wire. Several armature coils comprise a unit armature winding. The unit armature winding is wounded over the stator core side by side. The armature is divided into several phases. Each phase winding is switched by a half bridge circuit. To facilitate the understanding of the structure, a two-phase construction is shown in Fig. 2, but a multiphase construction could be employed to minimize pulsation of thrust as necessary. The adjoining unit armature winding of the same phase is connected inversely, and this connection type could decrease the inductance and improve the rate of current rise. The direct current from the power supply is switched over in correspondence with the position of superconducting magnets and alternately supplied to the armature coil as a square wave current, as shown in Fig. 3.

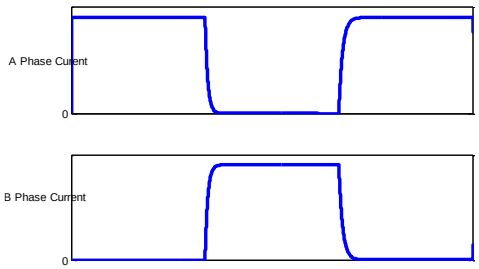

Fig.3. Current Wave Form of Armature.

3. DYNAMICS EQUATION

According to the ampere force formula, the armature coil current element $Id\boldsymbol{l}$ interacts with the superconducting magnetic field $\boldsymbol{B}$, the coil current element obtains the electromagnetic force

$$\vec{F} = I\vec{l} \times \vec{B} \tag{1}$$

But the magnetic field of an air core superconducting magnet is not uniform. The result of (1) is not accurate to

describe the relationship between thrust and position of the superconducting magnet. A SDCLM is constructed without ferromagnetic materials. Energy transformation takes place between superconducting coil and armature coils. A simple model for a superconducting coil and an armature coil is shown in Fig. 4. The magnetic energy between two coils can be expressed as

$$W' = \frac{1}{2} L_a {i_a}^2 + \frac{1}{2} L_s {i_s}^2 + M i_s i_a \tag{2}$$

So the magnetic energy of whole launch system is

$$W = \frac{1}{2} \sum_n L_a {i_a}^2 + \frac{1}{2} L_s {i_s}^2 + \sum_n M_n i_s i_a \tag{3}$$

Where L_a is the self-inductance of unit armature winding, L_s is the self-inductance of superconducting coils, M_n is the mutual inductance between superconducting coils and nth unit armature winding, i_s is the current of superconducting coils, i_a is the current of the armature coils.

The mechanical-electric coupling equation between superconducting coils and armature coils is

$$F_p = \frac{\partial W}{\partial x} = \sum_n \frac{\partial M_n}{\partial x} i_s i_a \tag{4}$$

The back-EMF induced by moving superconducting magnetic field can be expressed as follow

$$\begin{aligned} \varepsilon_a &= \sum_n \frac{\partial \psi_s}{\partial t} \\ &= \sum_n \frac{\partial M_n}{\partial t} i_{sc} = \sum_n \frac{\partial M_n}{\partial x} \frac{\partial x}{\partial t} i_{sc} = \sum_n \frac{\partial M_n}{\partial x} v i_{sc} \end{aligned} \tag{5}$$

Where ψ_s is the unit armature winding linkages, x is the superconducting magnet motion displacement, and v is the speed of carrier.

Armature coils can be described by an equivalent inductance circuit. V_0 is the voltage of the power and R_a is the resistance of the armature coils. The loop circuit equation of the armature coils is

$$R_a i_a + L_a \frac{di_a}{dt} + \varepsilon_a = V_0 \tag{6}$$

The motion equations of carrier are expressed by

$$a_l = \frac{F}{m_l} = \sum_n \frac{\partial M_n}{\partial x} \frac{i_s i_a}{m_l} \tag{7}$$

$$v = v_0 + \int_0^T a_l dt \tag{8}$$

$$x = x_0 + \int_0^T v dt \tag{9}$$

Where a_l is the acceleration of carrier and m_l is the mass of carrier.

Combing the mechanical-electric coupling equation, circuit equation, and the motion equations, the motion parameters of the SDCLM could be obtained.

The conversion efficiency of the system energy is defined as the ratio of carrier kinetic energy to the output energy of the power. The efficiency is expressed by

$$\eta = \int_o^T F_p x dt \Big/ \int_o^T V_0 i_a dt \tag{10}$$

4. ANALYSIS OF ARMATURE WINDING FORM

As shown in equation (4), the magnitude of the electromagnetic force of a linear motor is mainly related to the mutual inductance gradient of the armature coil and the excitation coil. And the thrust of the linear motor with different armature winding form can be compared by the mutual inductance gradient。In the coordinate in Fig. 4, the linear motor with air core structure can be simplified for two coils. Fig. 4(a) shows the ring winding structure and Fig. 4(b) shows the conventional winding structure. According to the theory of electromagnetism, in Fig.4 (a), the mutual inductance between two air core coils can be expressed as follow

$$\begin{aligned} M &= \frac{\mu_0}{4\pi} \oint_{l_1} \oint_{l_2} \frac{d\boldsymbol{l}_1 d\boldsymbol{l}_2}{r} \\ &= \frac{\mu_0}{4\pi} \oint_{l_1} \oint_{l_2} \frac{dxdx' + dydy' + dzdz'}{\sqrt{(x-x')^2 + (y-y')^2 + (z-z')^2}} \end{aligned} \tag{11}$$

(x,y,z) is the coordinate on superconducting coil, (x',y',z') is the coordinates on armature coil, l_1 is perimeter line of superconducting, and l_2 is perimeter line of armature coil. $(x_i,y_i,z_i,i=1,2,3,4)$ is the coordination of A、B、C、D, and $(x'_j,y'_j,z'_j,j=1,2,3,4)$ is the coordination of、B'、C'、D'. These points describe the perimeter line l_1 and l_2. Equation (11) can be solved as follow

$$\begin{aligned} M &= \frac{\mu_0}{4\pi} \oint_{l_1} \oint_{l_2} \frac{d\boldsymbol{l}_1 d\boldsymbol{l}_2}{r} \\ &= \frac{\mu_0}{4\pi} \sum_{i=1}^{4} \sum_{j=1}^{4} (-1)^{i+j} \Gamma(z'_i, x'_i, y'_i, z_j, x_j, y_j) \end{aligned} \tag{12}$$

Where Γ is

$$\begin{aligned} &\Gamma(z'_i, x'_i, y'_i, z_j, x_j, y_j) \\ &= -(z'_i - z_j) \ln[(z'_i - z_j) \\ &+ \sqrt{(x_j - x'_i)^2 + (y_j - y'_i)^2 + (z_j - z'_i)^2}\,] \\ &+ \sqrt{(x_j - x'_i)^2 + (y_j - y'_i)^2 + (z_j - z'_i)^2} \end{aligned} \tag{13}$$

The mutual inductance between superconducting coil and a unit armature winding is

$$\begin{aligned} &M_{12} = \frac{\mu_0}{4\pi} \sum_k \sum_{i=1}^{4} \sum_{j=1}^{4} (-1)^{i+j} \Gamma(z'_{ki}, x'_{ki}, y'_{ki}, z_j, x_j, y_j) \\ &x'_{k1} = x'_{k2} = x'_{k3} = x'_{k4} = x'_1 + kd; \end{aligned} \tag{14}$$

Where k is the turn number of a unit armature winding, and d is the pitch of turn.

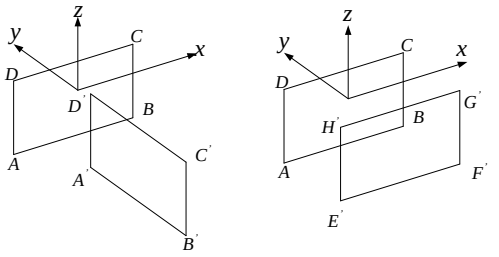

(a) Ring winding. (b) Conventional winding.

Fig.4. Two Types of Armature Winding

Similarly, the inductance and mutual inductance can be obtained as shown in Fig. 4 (b)

$$M'_{12}=\frac{\mu_0}{4\pi}\sum_{i}^{4}\sum_{j}^{4}(-1)^{i+j}\left[\psi(x_j,y_j,0;x'_i,y'_i,z')+\psi(y_j,x_j,0;y'_i,x'_i,z')\right] \quad (15)$$

Where

$$\psi(x,y,z;x',y',z')$$
$$=-(x-x')\ln[(x-x')+\sqrt{(x-x')^2+(y-y')^2+(z-z')^2}]+\sqrt{(x-x')^2+(y-y')^2+(z-z')^2} \quad (16)$$

Let A (-0.12,0,-0.15), C (0.12,0,0.15), A' (*x*,0.26,-0.15), C' (*x*,0.02,0.15), E'(-0.12+*x*,0.02,-0.15), G'(-0.12+*x*,0.02,0.15), x is the relative position of the two coils. The mutual inductance and mutual inductance gradient of two armature winding forms are shown in Fig. 5 and Fig.6. It can be seen from the figures that the mutual inductance and mutual inductance gradient of ring winding are both smaller than the conventional armature winding form, and the mutual inductance gradient peak value of conventional armature winding is about 2.5 times the ring armature winding form. In other words the electromagnetic thrust of linear motor with ring winding is smaller than the linear motor with conventional winding at the same electromotive force. This is because the air core linear motor lacks the ferry core to restrain the magnetic circuit, and the magnetic field diverges in the air. The closed magnetic field returns to the magnet through the armature winding effective edge and the upper and lower sides. The direction of electromagnetic thrust generated by the upper and lower armature side is opposite to the direction of electromagnetic thrust generated by the effective side, and this makes the motor output thrust small. But the ring winding density is high, it can increase the winding density to improve the thrust。In theory, in the case of the same current density, the wire load of the ring armature winding is 2 to 3 times larger than that of the conventional armature winding. Therefore, the electromagnetic thrust generated by the two kinds of air core armature winding linear motor is almost the same. However, the advantages of ring winding is in the low resistance and inductance, easy manufacturing and good heat dissipation。

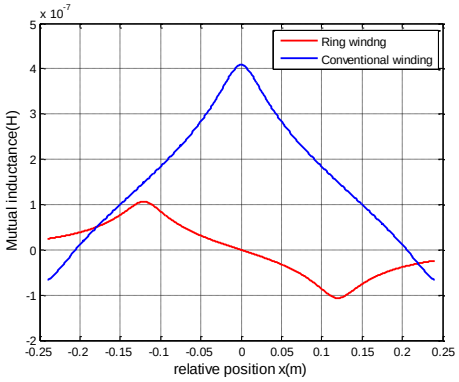

Fig.5. Mutual Inductance of Two Armature Winding Forms

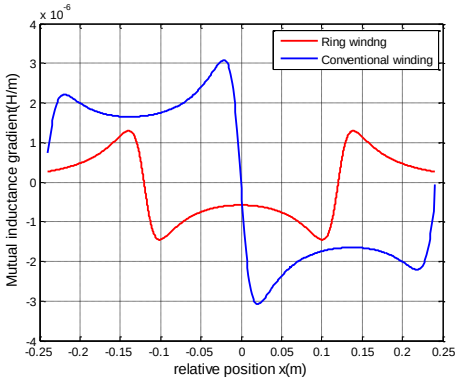

Fig.6. Mutual Inductance Gradient of Two Armature Windings

5. SIMULATION RESULTS

Static characteristic of the SDCLM is simulated with theoretical analysis and finite-element method (FEM) to analyze the performance.

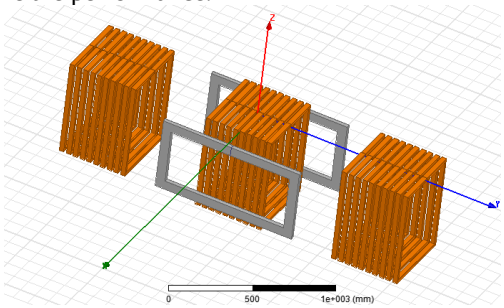

Fig.7. Finite-element Model of SDCLM.

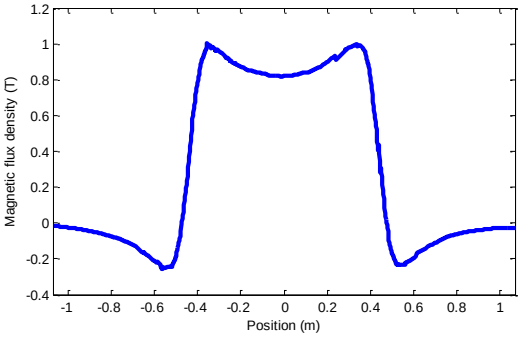

Fig.8. Magnetic Flux Density versus Position.

Table 1 Pertinent System Parameters

Superconducting magnet:	
Number of Superconducting Magnets	2
Section	Rectangle
Inner Rectangle	820mm×360 mm
Outer Rectangle	940mm×480 mm
Depth	25.4mm
Number of coil turns	2340
Current	210A
Unit of armature winding:	
Material	Copper
Overall dimension	453mm×640 mm
Depth	500mm
Conductor cross-section	30mm×20mm

The finite-element simulation model of SDCLM with three unit windings is shown in Fig. 7. The pitch of two unit armature windings is 940mm, and the gap between superconducting magnet and armature coils is 77.7mm. The number of a unit armature winding is 10, and the current of armature coils is 1000A. The pertinent system parameters are given in Table I. The coordinate system is located in the center of the middle unite armature winding. Fig. 8 shows the magnetic flux density versus position. The magnetic flux density is not uniform, and it would lead to the fluctuant thrust.

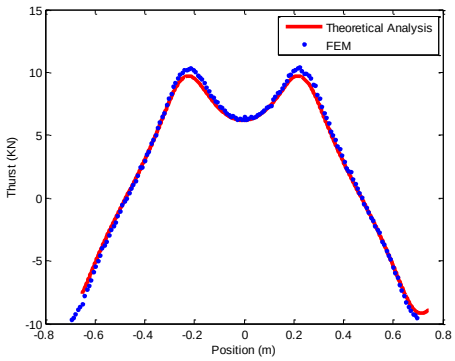

Fig.9. Static Thrust versus Position.

The results of theoretical analysis and finite-element method for the static thrust versus position are shown in Fig. 9. There is a good agreement between the results obtained with the two methods. It indicates that the SDCLM has a big thrust with large gap and low armature current.

To evaluate SDCLM system for the launcher application, the launch operation for the 1000 kg loading was simulated dynamically. Ten pairs of superconducting magnets are mounted on the carrier. The armature coils are two-phase construction. The unit armature windings of same phase are alternately connected in series. The armature track is 968 m long, and the track is segmented into two blocks for reducing resistance loss. The resistance and the inductance of a block are 0.6828Ω and 0.0118 H. The number of a unit armature winding is 20, and the operational current of armature coils is 1000 A. The voltage of the power is 60 KV. The launch velocity is 400 m/s. The loading is suspended by maglev system and the friction is neglected. The atmospheric drag is considered. The aerodynamic drag factor is 0.05, and the frontal area is 1 m^2. The pertinent system parameters are given in Table 1.

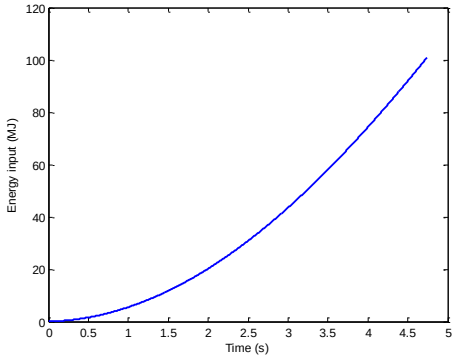

Fig.10. Energy Input versus Time.

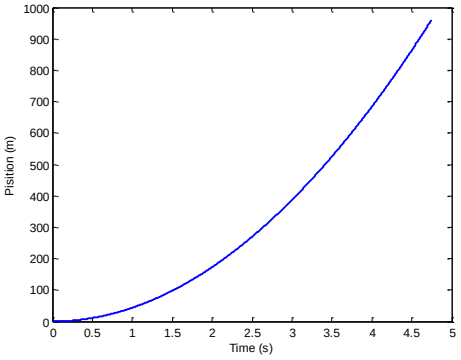

Fig.11.Position of Carrier versus Time.

Dynamic simulation results are shown as Figs. 10-13. Fig. 10 shows the energy input versus time, and the maximum energy input is 101 MJ. Fig. 11 shows the displacement of carrier. The launch displacement is 959.3 m. Fig. 13 is the curves of magnetic thrust versus time. And the energy efficiency versus time is shown in Fig.12. The energy efficiency is 81.37% when the carrier receives the 400 m/s. and it could reach the higher energy efficiency by decreasing armature current and increase armature turns. As shown in Fig. 13, the magnetic thrust fluctuation range is from 70 KN to 105 KN because of nonuniform magnetic flux density, and there is a mutation thrust at the point A. The mutation thrust is caused by commutation.

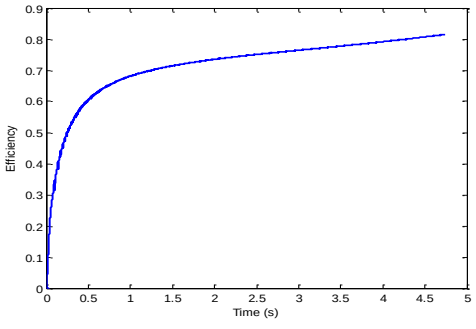

Fig.12. Energy Efficient versus Time.

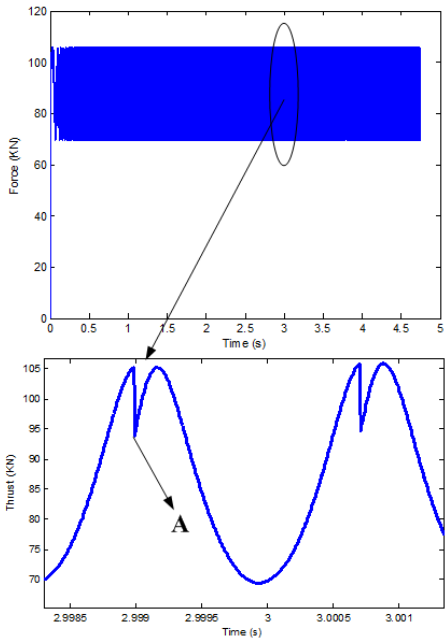

Fig. 13.Electromagnetic Thrust versus Time.

6. THRUST CONTROL BASED ON CURRENT COMPENSATION

The thrust control of SDCLM is realized by the current compensation control and current loop control. The control can be decomposed into two steps: First, the current compensation controller is designed to commutation thrust fluctuation to improve the performance of SDCLM. Then, the current loop is designed to improve the system's rapidity. The overall design is shown in Figure 14.

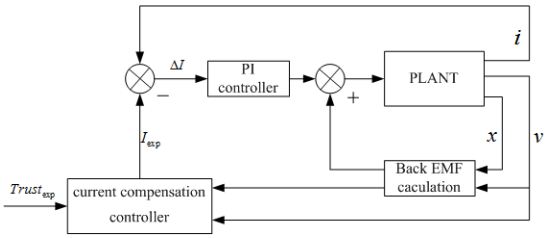

Fig 14.Control Block Diagram

The current is alternately supplied to the two phase winding, when the A phase is excited, the thrust is expressed

$$F_p = \sum_n \frac{\partial M_{an}}{\partial x} i_s i_a = \frac{\varepsilon_a i_a}{v} \tag{17}$$

Equation (17) shows the magnetic thrust is related to the gradient of mutual, the current of the superconducting magnet and armature current. Superconducting magnet is constant current. So the fluctuant of the thrust is caused by gradient of mutual and armature current. Figure 15 shows the mutual gradient between superconducting coils with air core and armature coils. The thrust fluctuant is caused by nonuniform mutual gradient. But the mutual gradient could be calculated, so current wave forms can be found to suppress the fluctuant thrust. The back-EMF is evaluated by equation (17), the velocity is achieved by positioning system and the expected current is obtained

$$i_{a\exp} = \frac{F_{\exp} v}{\varepsilon_a} \tag{18}$$

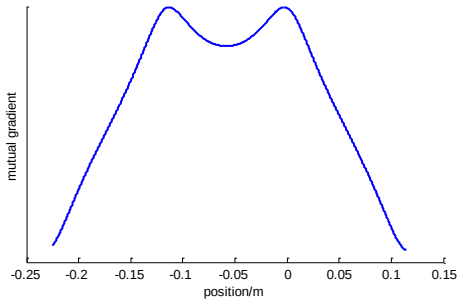

Fig. 15.Mutual Gradient versus Position

Then the current loop is designed. Power circuit is the inverter link, and its transfer function can be equivalent to a first-order inertia. Thus, the current loop control structure shown in Fig. 16 can be obtained. In the figure, ε is the back EMF; t_V is the inverter's equivalent time constant; k_V is the inverter's voltage output proportional coefficient.

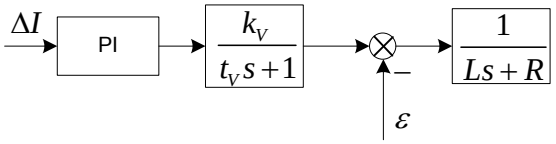

Fig 16. Current Loop Structure

When the current loop controller is designed, the influence of back EMF can be neglected. The current loop object transfer function is:

$$G(s) = \frac{k_V}{(t_V s+1)(Ls+R)} \tag{19}$$

Assuming that the PI controller's proportional and integral coefficients are k_P and k_I, then the controller's transfer function can be expressed as (20)

$$\frac{k_P s + k_I}{s} \tag{20}$$

To reduced-order model, let $\frac{k_P}{k_I} s+1 = \frac{L}{R} s+1$, then the open-loop transfer function can be presented as:

$$G(s) = \frac{k_I k_V}{R} \frac{1}{s(t_V s+1)} \tag{21}$$

The control of the current loop generally requires fast tracking while ensuring that the overshoot of the step response is small. When the parameter design satisfied the overshoot of the current step response will be 4.3% and it will have a faster response.

$$\frac{k_I t_V k_V}{R} = 0.5 \tag{22}$$

By (20) and (22), the proportional and integral coefficient of PI controller can be obtained.

The parameters of SDCLM are shown in TABLE I. The

thrust control based on current compensation and the traditional rectangular current control is simulated by matlab. And the thrust curve and a phase current curve versus time is shown in Figure 17 and Figure 18. Figure 17 shows current compensation control is useful to suppress thrust fluctuant.

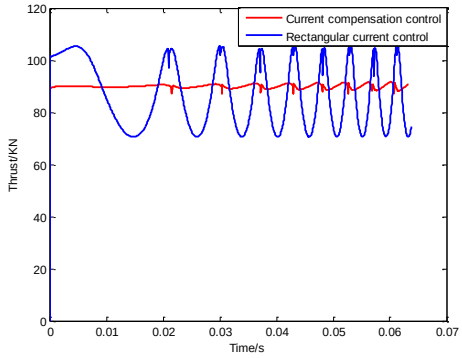

Fig 17.The Thrust Curve versus Time

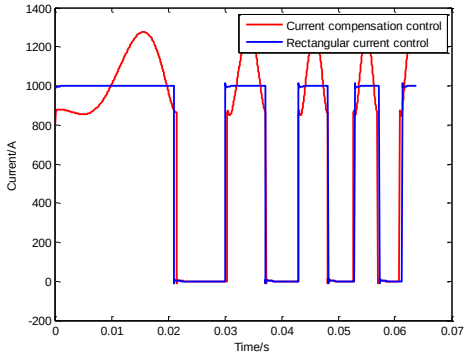

Fig 18.The A Phase Current versus Time

7. CONCLUSIONS

Conceptual design and operation principle of SDCLM have been presented in this paper. In addition to theoretical model, finite-element methods have been used to confirm the computational accuracy. To evaluate SDCLM for the launcher application, the combined electro-mechanical system was simulated dynamically through a launch to verify its performance. The simulation results indicate that SDCLM have high energy efficiency with large mass launch and super velocity. Moreover the gap of the motor is large, and it is more appropriate for superhigh velocity launch. And a thrust control of SDCLM based on current compensation has been presented. For the evaluated back-EMF shape, implementable current wave forms can be calculated that minimize thrust fluctuant. Simulation results shows current compensation controller is useful to suppress thrust fluctuant. In the future, it could be used in launch assistance for space vehicles and high speed test track propulsion.

However, when the two-phase armature is switched, it still cause a mutation thrust. To improve the magnetic thrust performance, a multiphase construction and advance commutation control strategies should be adopted.

REFERENCES

[1] Skurdal D. B., Randy L. G., 2009. Multimission electromagnetic launcher, IEEE Trans. Magn., 45(1): 458-461. 10.1109/TMAG.2008.2008551

[2] Patterson D., Monti A., Brice C. et al., 2002. Design of a linear bulk superconductor magnet synchronous motor for electromagnetic aircraft launch system, in Proc. 37th IAS Annual Meeting, 1950-1957. 10.1109/TASC.2004.824342

[3] Stumberger G., Mehmet T. A., Damir Z. et al., 2004. Design of a linear bulk superconductor magnet synchronous motor for electromagnetic aircraft launch, IEEE Trans. Appl. Superconduct., 14(1): 54-62.10.1109/TASC.2004.824342.

[4] Doyle M. R., Samuel D. J., Conway T.,et al. 1995. Electromagnetic aircraft launch system-EMALS, IEEE Trans. Magn., 31(1): 528-533.10.1109/20.364638.

[5] Cho H. W., Sung H.-K., Sung S.Y., et al. 2008. Design and characteristic analysis on the short-stator linear synchronous motor for high-speed maglev propulsion, IEEE Trans. Magn., 44(11):4369-4372.10.1109/TMAG.2008.2001511.

[6] Jin H. L., Jeongmin J., Youngjae H., et al., 2014. Development of the linear synchronous motor propulsion tested for super speed maglev, in Proc. 16th ICEMS, 1936-1938.10.1109/ICEMS.2013.6713223.

[7] Sen P., 1975. On linear synchronous motor (LSM) for high speed propulsion, IEEE Trans. Magn., 11(5): 1484-1486.10.1109/TMAG.1975.1058873.

[8] Jun E., 2004. The novel power supply system in the yamanashi maglev test line, in Proc. 18th 21th International Conference on Magnetically Levitaion System and Linear Drives, 451-454.

[9] Sakamoto, Shigeru, Hiroyuki W., et al. 1997. Development of a maglev superconducting magnet for the Yamanashi test line in Japan vibration characteristics and analysis for design, IEEE Trans. Appl. Superconduct., 7(3):3791-3796. 10.1109/77.622976.

[10] Kazuo S., 1996. Development of magnetically levitated high speed transport system in Japan, IEEE Trans. Magn., 32(4):2230-2235.10.1109/20.508609.

[11] Kaiji S., Tadashi H., 2014. High-speed positioning of ultrahigh-acceleration and high-velocity linear synchronous motor, International Journal of Precision Engineering and Manufacturing, 15(8):1537-1544. https://doi.org/10.1007/s12541-014-0502-y.

[12] Turman B. N., Marder B. M., Rohwein G. J., et al, 1995. The pulsed linear induction motor concept for high-speed trains, Sandia National Laboratiories, Livermore, SNL, Rep. SAND95-1268.10.2172/90379.

[13] Takahashi N., 2011. Development of Ground Coil Type of PLG for Maglev, in Proc. 21th International Conference on Magnetically Levitaion System and Linear Drives.

[14] Zhi H. W., Jian X. J., 2014. Characteristic Analysis of HTS Linear Synchronous Generators Designed With HTS Bulks and Tapes, IEEE Trans. Appl. Superconduct., 24(5):1-5.10.1109/TASC.2014.2344766

[15] Luo W.B., Wang Y., Gui Z.X., et al., 2013. Connection Pattern Research and xperimental ealization of Single Stage Multipole Field lectromagnetic Launcher, IEEE Trans. Magn., 41(11):3173-3179.10.1109/TPS.2013.2281240.
[16] Wang S.Z., 2014. The homopolar machine principle applied in ectromagnetic aircraft launch system, Ship Science and Technology, 36(9):150-152.
[17] Umemori T., Kawashima M., Oda M., et al.,1979. Development of DC Lenear Motor - Fundamental Construction and Feasibility, Transactions on Power Apparatus and Systems, 98(4):1456-1465.10.1109/TPAS.1979.319348.
[18] Daniel A. B., 2010. Holloman High Speed Test Track Maglev Program Update, Holloman Air Force Base, Nashville, AFB, Rep, AIAA 2010-1707.https://doi.org/10.2514/6.2010-1707 .
[19] Hooser M. D., 2010. Holloman High Speed Test Track Magnetically Levitated (MAGLEV) Sled Six Degree-of-Freedom Model, Holloman Air Force Base, Nashville, AFB, Rep, AIAA 2010-1706.
[20] Su Y.H., Langhorn A., Ketchen D., et al., 2009 Magnetic Levitation Upgrade to the Holloman High Speed Test Track, IEEE Trans. Appl. Superconduct., 19(3):2074-2077.10.1109/TASC.2009.2019558.
[21] Su Y.H, Ketchen D., Holland L., Status of the Magnetic Levitation Upgrade to Holloman High Speed Test Track, in Proc. 20th Intern Conf on Magnetically Levitated Systems and Linear Drives.https://doi.org/10.2514/6.2000-2289.
[22] He J.L., Howard C., 1997. Magnetic damping forces in figure-eight-shaped null-flux coil suspension systems, IEEE Trans. Magn., 33(5):4230-4232.10.1109/20.619719.
[23] Haney J.W., Lenzo J., 1996. Issues Associated With A Hypersonic Maglev Sled, in Proc. 3rd International Symposium on Magnetic Suspension Technology, 607-621.https://ntrs.nasa.gov/search.jsp?R=19960050141.